Simulation of the AX and BX transition emission spectra of the InBr molecule for diagnostics in low-pressure plasmas

S Briefi, U Fantz

Simulation of the A − X and B − X transition emission spectra of the InBr molecule for diagnostics in low pressure plasmas

S Briefi[1] **and U Fantz**[1,2]

[1]Lehrstuhl für Experimentelle Plasmaphysik, Institut für Physik, Universität Augsburg, Universitätsstraße 1, D-86135 Augsburg, Germany
[2]Max-Planck-Institut für Plasmaphysik, EURATOM Association, Boltzmannstr. 2, D-85748 Garching, Germany

E-mail: `stefan.briefi@physik.uni-augsburg.de`

Abstract. Inductively coupled low pressure discharges containing InBr have been investigated spectroscopically. In order to obtain plasma parameters such as the vibrational and rotational temperature of the InBr molecule, the emission spectra of the A $^3\Pi_{0^+} \rightarrow$ X $^1\Sigma_0^+$ and the B $^3\Pi_1 \rightarrow$ X $^1\Sigma_0^+$ transitions have been simulated. The program is based on the molecular constants and takes into account vibrational states up to $v = 24$. The required Franck-Condon factors and vibrationally resolved transition probabilities have been computed solving the Schrödinger equation using the Born-Oppenheimer approximation. The ground state density of the InBr molecule in the plasma has been determined from absorption spectra using effective transition probabilities for the A − X and B − X transition according to the vibrational population. The obtained densities agree well with densities derived from an Arrhenius type vapour pressure equation.

PACS numbers: 52.70.Kz, 33.20.Lg, 33.20.Vq, 33.70.Ca, 33.70.Fd

Submitted to: *J. Phys. D: Appl. Phys.*

1. Introduction

Metal halides such as InBr are discussed to be an efficient molecular radiator in low pressure plasmas. Up to now, rare gas discharges containing mercury in the high and low pressure range are commonly used for lighting purposes. Several properties of mercury are hereby utilized such as a high vapour pressure and the strong and efficient radiation in the visible and especially the ultraviolet spectral range. Recent research both in low and high pressure lamps ([1, 2, 3] and [4, 5]) focuses on finding efficient substitutes for mercury due to its toxicity. Molecular radiation - especially from metal halides - is under discussion to be a good alternative to mercury [6]. Some of the suggested molecules are already used as additives in common high pressure lamps to achieve a higher colour

rendering index [7]. The performance of low pressure discharges containing indium halides (InCl, InBr and InI) has been investigated recently [8, 9]. The most intense emission bands of their molecular spectrum are in the near UV range (330 - 420 nm) which makes the conversion into visible light by a phosphor more efficient compared to mercury in fluorescent lamps due to the lower Stokes shift. These emission bands consist of transitions from the first two excited states to the ground state: A $^3\Pi_{0^+} - $ X $^1\Sigma_0^+$ and B $^3\Pi_1 -$ X $^1\Sigma_0^+$. The minima of the potential curves of the InBr molecule are at 3.30 eV for the A state and at 3.39 eV for the B state [10]. The resulting band spectrum is in the wavelength range between 350 and 400 nm. It is still under discussion if the third electronic state, the C $^1\Pi_1$ state, is bound or repulsive [11]. The C $-$ X band emission is discussed to be around 285 nm [12]. A plasma which contains InBr (ionization energy $E_{\mathrm{Ion}}(\mathrm{InBr}) = 9.41$ eV [13]) also emits intense radiation from indium in the blue spectral range at 410.18 nm and 451.13 nm due to the dissociation of the molecule (dissociation energy of InBr $D_{\mathrm{e}} = 3.99$ eV [10]).

InBr has a very low vapour pressure at ambient temperature [8]. To obtain a significant partial pressure of InBr in a plasma, the discharge vessel has to be heated up to several hundred degrees centigrade. The amount of InBr in the plasma which strongly influences the intensity of the molecular emission is determined by the temperature of the coldest spot of the vessel wall.

For lighting purposes, the aim is to maximize the molecular near UV radiation of a rare gas plasma containing InBr at a fixed discharge power. Therefore it is important to investigate the population mechanisms of the involved electronic states in the molecule. The vibrational and rotational population of the electronic states determine the shape of the molecular band spectrum and, as the single vibrational levels have different radiative lifetimes, also the intensity of the emission. A well-known example of these characteristics are nitrogen bands [14]. Spectroscopic diagnostics are common techniques to determine the influence of external parameters such as pressure, power and heating temperature on the population densities and on the emission respectively. For InBr, however, the vibrational and rotational population cannot be obtained from an analysis of individual lines from the measured spectrum because of the manifold of overlapping ro-vibrational lines of the two electronic transitions.

The aim of this paper is to determine the rotational and vibrational population of the molecule from emission spectra by comparing the measured relative intensity of the band with simulated spectra. With the knowledge of these populations the ground state density of InBr can be obtained from absorption spectroscopy measurements. First, the simulation procedure will be described. The required Franck-Condon factors and vibrational resolved transition probabilities of InBr have not been available in literature and were determined numerically. Examples of simulated spectra with different spectral resolution of the optical system and with varying vibrational and rotational temperatures are given in section 2.4. Section 3 describes the application to low pressure plasmas and presents the results together with a discussion on the accuracy of the determination of the vibrational and rotational temperature. In addition, the

ground state density of InBr obtained from absorption measurements is compared with the density calculated from an Arrhenius type vapour pressure equation.

2. Simulation of InBr emission spectra

The band spectrum of InBr between 350 and 400 nm arises from overlapping emission of the electronic A − X and B − X transition and can be seen easily in the measurements presented in section 3. The C − X band spectrum could not be observed. However, it does not contribute to the near UV radiation and, therefore, the focus is put on the A − X and B − X transition. Due to the large mass of InBr (atomic weight 194.722 u) the molecular constants and hence the energy differences between vibrational and rotational states characterized by their quantum numbers v and J are very small ($\Delta E_v \approx 0.03$ eV, $\Delta E_J \approx 3 \cdot 10^{-5}$ eV). States with high quantum numbers v and J can be populated with rather small amounts of energy and many emission lines occur in a narrow wavelength range. Due to the Doppler broadening of emission lines it is only possible to resolve the structure of the sequences (transitions with fixed $\Delta v = v' - v''$) of the band spectrum even with a high resolution spectrometer ($\Delta\lambda_{\mathrm{FWHM}} \approx 25\ pm$). This is demonstrated in Figure 1 which already shows simulated spectra with a FWHM of the apparatus profile of 25 pm. The simulation was performed using the procedure described in the following section.

2.1. Computing method

As the energy difference between the individual states is very low, it is necessary to take into account states with high vibrational and rotational quantum numbers for the X, A and B state. First investigations showed that it is sufficient for a good match of simulated and measured spectra to limit the calculation to the energetically lowest 25 vibrational states and 300 rotational states in each electronic state. Significant deviations have been observed by reducing the vibrational quantum number below $v = 20$. The energy of the rovibrational states of the X, A and B state is calculated using the molecular constants taken from [10]. The wavelength of a transition from the upper electronic state i (A or B) with vibrational and rotational quantum numbers v' and J' to the lower state k (the ground state X) with v'' and J'' is derived from the energy difference of the states.

The relative vibrational population of the ground state is calculated assuming a Boltzmann distribution with the vibrational temperature T_{Vib}. This assumption is reasonable due to the small energy difference between the vibrational states (about 0.03 eV). For the excited states, the relative vibrational population $n_i^{v'}$ is derived from the population of the ground state applying the Franck-Condon principle [15]. To obtain the relative population $n_{i,v'}^{J'}$ of the rotational states with the vibrational quantum number v' of the excited electronic states, again a Boltzmann distribution characterized by the rotational temperature T_{Rot} is used. The relative population of a single state with v'

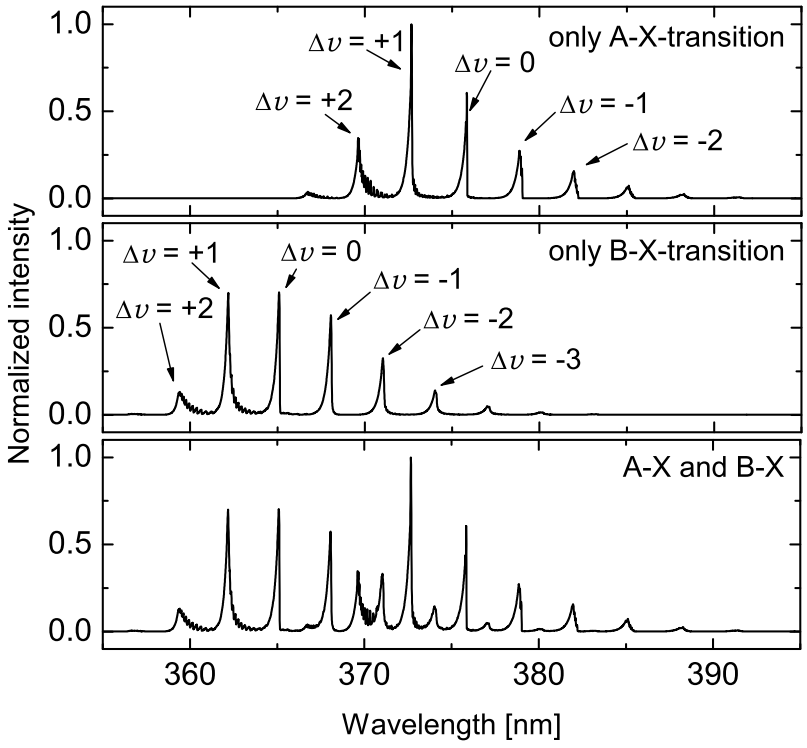

Figure 1. Simulated emission spectra of InBr. Upper part: only A − X transition; center: only B − X; bottom part: both transitions. The most intense vibrational sequences of each transition are annotated.

and J', $n_i^{v',J'}$, is then given by

$$n_i^{v',J'} \propto n_i^{v'}(T_{\mathrm{Vib}}) \cdot n_{i,v'}^{J'}(T_{\mathrm{Rot}}). \tag{1}$$

The relative populations are normalized that the population of the whole electronic state is equal to unity:

$$\sum_{v'} n_i^{v'} = 1 \quad \text{and} \quad \sum_{J'} n_{i,v'}^{J'} = n_i^{v'}. \tag{2}$$

According to [16] the relative intensity $I^{ik,v'v'',J'J''}$ of the transition $(i, v', J') \rightarrow (k, v'', J'')$ is determined by

$$I^{ik,v'v'',J'J''} \propto \frac{\nu}{d_i}\, n_i^{v',J'}\, A_{ik}^{v'v''}\, S_{\mathrm{P,Q,R}}(J'), \tag{3}$$

where ν denotes the frequency of the emitted photon, d_i the degeneracy, $n_i^{v',J'}$ the population density in the state i and $A_{ik}^{v'v''}$ the vibrationally resolved transition probability. $S_{\mathrm{P,Q,R}}(J')$ is the Hönl-London factor for the P,Q or R branch, which describes the intensity of the emission line depending on the rotational quantum numbers of the states involved [16]. The Hönl-London factors depend on the Hund's coupling

cases of the electronic states which are involved in the transition. As InBr is a very heavy molecule Hund's case (c) is valid for both the A − X and the B − X transition [10]. Furthermore, both transitions are singlet − triplet transitions which means spin-orbit interactions may lead to perturbations in the intensity distribution of rotational lines [17]. The exact formulae for the Hönl-London factor for the A − X and B − X transition can be found in [17]. They contain constants which describe the magnitude of perturbation due to the spin-orbit interaction. In the case of InBr, these constants are not available in literature. Therefore the Hönl-London factors of Hund's case (a) are used in the simulation as an approximation since the resultant angular momentum from the coupling of the single electronic and rotational angular momenta for the electronic state is the same as in case (c) [16]. Thus, the spin-orbit interactions are neglected. The comparison of simulated spectra to measurements has to demonstrate the validity of this approximation.

For each transition line a Gaussian line profile is calculated with the peak of the profile at the wavelength of the transition and folded with the relative intensity of the line emission. The FWHM of the line profile is an input parameter of the simulation. As only low pressure plasmas are investigated the dominating line broadening mechanism is the Doppler broadening. Due to the large mass of the InBr molecule the FWHM of the Doppler profile is still much smaller than the apparatus profile of the optical system. Therefore the FWHM used for the simulation is given by the experimental setup. It is determined by utilizing the nearby indium lines. To obtain a spectrum, the intensities of all computed lines are added up. The relative intensities of the two electronic transitions can be adjusted separately to consider the possibility of a different electronic population of the A and the B state.

The InBr molecule basically consists of two relevant isotopic species, ^{115}In^{79}Br with natural abundance of 48.51% and ^{115}In^{81}Br with 47,19%. Therefore the emission is simulated separately for both species and then added, taking into account the natural abundances to obtain the final spectrum. The isotopes ^{113}In^{79}Br (2,18%) and ^{113}In^{81}Br (2,12%) are neglected due to their low abundance.

2.2. Franck-Condon factors and transition probabilities

The simulation requires vibrationally resolved Franck-Condon factors (FCF) and transition probabilities $A_{ik}^{v'v''}$ as input parameters. FCF of the InBr molecule can be found in literature only for vibrational quantum numbers up to $v = 13$ [18] and radiative lifetimes can be found only for selected vibrational levels of the A or B state [8]. Therefore FCF and $A_{ik}^{v'v''}$ were calculated using the program TraDiMo [19]. This program derives the eigenvalues and vibrational wave functions via numerically solving the Schrödinger equation. The calculations are based on the Born-Oppenheimer potential curves, the electronic dipole transition moments and the reduced mass of the molecule as input parameters. The overlap integral of two vibrational wave functions in different electronic states yields the FCF. The $A_{ik}^{v'v''}$ are calculated from the overlap of

the vibrational wave functions with the electronic dipole transition moments. A more detailed description of TraDiMo can be found in [19].

There are three complete sets of potential curves for the X, A and B state of InBr available in literature: RKR potential curves [18], Hulburt-Hirschfelder potential curves [20] and potential curves from MRDCI calculations [11]. The RKR potential curves are only given for vibrational quantum numbers up to $v = 12$. As already mentioned, for a good match of the simulated spectrum and the measurement vibrational states up to $v = 24$ have to be taken into account. Hence, Morse potential curves were calculated using the molecular constants of InBr [10] which reproduced the RKR potential curves quite well. Morse potential curves are a very good approximation close to the minimum of the potential curve and therefore for low vibrational energies. The energy of the state with vibrational quantum number $v = 24$ of InBr is still rather low due to the large mass of the molecule. TraDiMo calculations were carried out with all three sets of potential curves: with the Morse potential curves as extended fit to the RKR curves, with the Hulburt-Hirschfelder curves and with those from the MRDCI calculations. The electronic dipole transition moments $D_{AX}(r)$ and $D_{BX}(r)$ for the A − X and B − X transition are taken from [8]. They are empirically determined and given as:

$$\begin{aligned} D_{AX}(r) &= D_{AX}(r_{eX}) \left(1 + 4 \cdot \left(\frac{r}{r_{eX}} - 1\right)\right) \\ D_{BX}(r) &= D_{BX}(r_{eX}) \end{aligned} \tag{4}$$

where r_{eX} is the equilibrium nuclear distance of the ground state and with $D_{AX}(r_{eX}) = 0.0705$ a.u. and $D_{BX}(r_{eX}) = 0.053$ a.u.. As the different potential curves deviate from each other the obtained sets of FCF and $A_{ik}^{v'v''}$ also show deviations. Simulations were carried out with all sets of data and compared to measured emission spectra. The best results by far regarding the match of the relative intensity of simulated and measured spectra were achieved with the data derived from the Morse potential curves.

Uncertainties of the FCF or transition probabilities are determined by the accuracy of the input parameters (potential curves and electronic dipole transition moments). If the potential curves vary slightly, different absolute values of the vibrational eigenvalues are computed [19]. Small changes of the eigenvalues lead to deviations in the wave functions and hence to differences in the FCF. The deviation depends on the absolute value of the FCF and transition probabilities (the smaller the absolute value, the larger the deviation) which means the precision is rather determined by the digit than a percentaged value [19].

Since the Morse potential curves depend on molecular constants, slightly different curves are obtained for the isotopic species. Calculations of the FCF and $A_{ik}^{v'v''}$ have been carried out on the one hand with the mass of both relevant isotopes (^{115}In^{79}Br and ^{115}In^{81}Br) and on the other hand with the averaged mass. The simulation of the band spectrum using either the data gained considering the isotopic species or the averaged mass only differ in the range of a few percent. So, for simplicity Franck-Condon factors and transition probabilities derived with the average mass are used for the simulation of

the relative intensity. These FCF and $A_{ik}^{v'v''}$ can be found in the tables A1 to A8 in the Appendix. Considering the uncertainty discussion above, all calculated Franck-Condon factors that are smaller than $1 \cdot 10^{-5}$ and all transition probabilities smaller than 1 s^{-1} are replaced by zero.

In [18] FCF up to $v = 13$ of the A − X and B − X transition of InBr are calculated using the RKR potential curves published in the same paper. Table 1 compares the FCF calculated via TraDiMo to the data taken from [18], which is denoted in brackets, up to a vibrational quantum number of $v'' = v' = 3$ for the A − X transition. Even though the Morse potential curves used for the TraDiMo calculations reproduce the RKR curves well the potential curves diverge slightly. As discussed above, this leads to differences in the calculated FCF. However, it can be seen that for the relevant Franck-Condon factors (high absolute values) the difference is only a few percent. The same consideration is valid for the FCF of the B − X transition.

Table 1. Comparison of the derived FCF to the data taken from [18] (in brackets) for the first four vibrational states in the A − X transition.

$v' \rightarrow v''$	$v'' = 0$	$v'' = 1$	$v'' = 2$	$v'' = 3$
$v' = 0$	0.581 82 (0.6030)	0.293 43 (0.2841)	0.094 45 (0.0861)	0.024 06 (0.0211)
$v' = 1$	0.343 17 (0.3273)	0.136 01 (0.1538)	0.279 79 (0.2863)	0.161 57 (0.1562)
$v' = 2$	0.069 79 (0.0644)	0.407 45 (0.4010)	0.011 62 (0.0135)	0.193 27 (0.2000)
$v' = 3$	0.005 10 (0.0052)	0.148 56 (0.1442)	0.371 48 (0.3628)	0.003 81 (0.0058)

Table 2 shows a comparison of the calculated radiative lifetimes of a vibrational level $\tau_{v'}^{i} = \left(\sum_{v''} A_{ik}^{v'v''}\right)^{-1}$ with those available in literature [8]. The lifetimes differ slightly, but unfortunately in [8] no specification of the input data of the calculation and no details about the calculation itself is given.

Table 2. Calculated radiative lifetimes $\tau_{v'}^{i}$ of selected vibrational levels for two electronic states. For comparison, the values taken from [8] are denoted in brackets.

State	A	B
$v' = 0$	6.81 μs (6.4 μs)	9.24 μs (8.7 μs)
$v' = 10$	4.55 μs (4.5 μs)	9.20 μs (9.3 μs)

2.3. Effective transition probabilities

The determination of the population density of the electronic states of InBr with spectroscopic measurements requires the knowledge of the effective transition probability A_{ik}^{eff}, where i denotes the A or B state and k the X state. It can be obtained by weighting the inverse lifetimes of the single vibrational levels $\left(\tau_{v'}^{i}\right)^{-1} = \sum_{v''} A_{ik}^{v'v''}$ with a vibrational

population according to Boltzmann:

$$A_{ik}^{\mathrm{eff}}(T_{\mathrm{Vib}}) = \sum_{v'} \left[\left(\sum_{v''} A_{ik}^{v'v''} \right) \cdot n_i^{v'}(T_{\mathrm{Vib}}) \right] \quad \text{with} \sum_{v'} n_i^{v'}(T_{\mathrm{Vib}}) = 1. \tag{5}$$

The vibrational temperature is taken from the fit of the simulated spectrum to the measurement. Table 3 shows effective transition probabilities calculated with different T_{Vib}. It can be seen that the A_{ik}^{eff} for the A − X transition (which has a electronic dipole transition moment varying over the internuclear distance [8]) changes with increasing vibrational temperature whereas for the B − X transition (which has a constant electronic dipole transition moment [8]) the A_{ik}^{eff} is almost constant.

Table 3. Effective transition probabilities A_{ik}^{eff} calculated for different vibrational temperatures.

T_{Vib} (K)	$A_{\mathrm{AX}}^{\mathrm{eff}}$ (10^5 s^{-1})	$A_{\mathrm{BX}}^{\mathrm{eff}}$ (10^5 s^{-1})
400	1.560	1.084
600	1.603	1.084
800	1.647	1.085
1000	1.692	1.085
1200	1.736	1.084
1400	1.776	1.083

2.4. Influence of input parameters on simulated spectra

With the simulation program it is now possible to determine the influence of the vibrational and rotational temperature on the structure of the emission band. Furthermore, spectra simulated with a rather wide FWHM of the line profile (1 nm, low resolution, typical for a broad band spectrometer) can be compared to those calculated with the same parameters but a narrow FWHM of 0.025 nm (high resolution spectrometer). Figure 2 shows simulated spectra with fixed T_{Vib} and two different T_{Rot} for low and high spectral resolution. Rotational temperatures of 500 K and 1000 K are used as this temperature range is typical for low pressure plasmas. In case of the low resolution spectra the rotational temperature hardly changes the structure of the band. Even for low T_{Rot} the sequences are overlapping strongly. In the case of high resolution the spectrum simulated with higher rotational temperature shows a distinct broadening of the single sequences which overlap only slightly.

Varying the vibrational temperature with low spectral resolution leads to a strong change of the relative intensity of the sequences and to a slight broadening of the sequences. This can be seen in figure 3. The change in the relative intensity can also be seen with high resolution. However, the broadening can now be identified to be caused by the population of states with higher vibrational quantum number in the

case of increased vibrational temperature. Transitions from higher vibrational quantum number are located in the shoulder of the single sequences. This leads to a broadening of the whole sequence in spectra calculated with low resolution as these transitions cannot be resolved. With high resolution, these transitions occurring with high vibrational temperature can be seen at 360 and 370 nm, for example.

Thus, a measurement with a high resolution is advantageous for the determination of the vibrational and the rotational temperature of the InBr molecule. All measurements presented in this paper are carried out with a high resolution spectrometer with a FWHM of the apparatus profile of 25 pm.

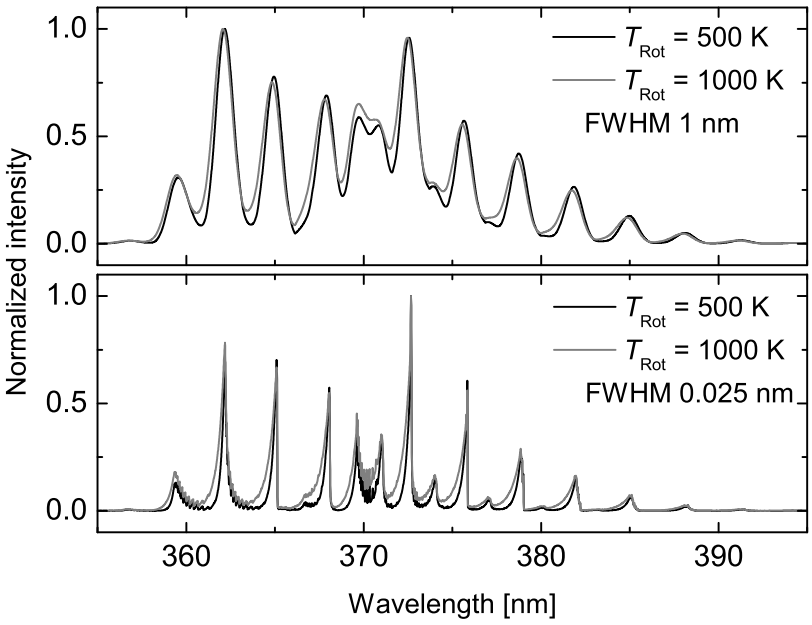

Figure 2. Simulated emission spectra with varying T_{Rot} for low (upper part) and for high spectral resolution (bottom part). T_{Vib} is fixed at 1000 K.

3. Applications to low pressure plasmas

3.1. Experimental setup

Rare gas discharges containing InBr have been generated via inductively RF-coupling at a frequency of 13.56 MHz and a generator power of 100 W in sealed cylindrical quartz cells. These cells are filled with a few mg InBr salt and Helium or Argon at a pressure of a few mbar. As InBr has a very low vapour pressure at ambient temperature, the whole cell was heated up to several hundred degrees centigrade using hot air flowing through a heat container. The amount of InBr in gas phase and in

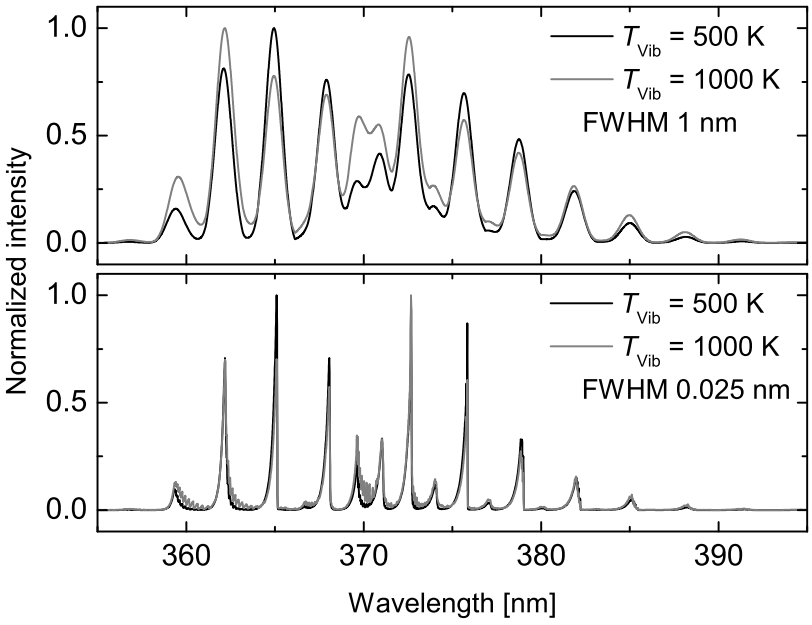

Figure 3. Simulated emission spectra with varying T_{Vib} for low (upper part) and for high spectral resolution (bottom part). T_{Rot} is fixed at 500 K.

the plasma is determined by the coldest spot of the wall of the cell which is not well-defined. The temperature of the hot air inside the heat container is measured with three thermocouples which are placed on the left, in the middle and on the right part of the heat container. The heating temperature T_{H} of the vessel is defined as the averaged measured temperatures of the three thermocouples. Figure 4 shows a schematic view of the experimental setup. The line-of-sight (LOS) for optical emission and absorption spectroscopy is axial (radial centered). A high resolution spectrometer with a focal length of 750 mm, a 1800 lines/mm grating and a CCD detector resulting in a FWHM for the apparatus profile of 25 pm is used. For white light absorption measurements a stabilized high-pressure Xe-lamp (450 W) is applied.

3.2. Comparison of measurements with simulation

Measurements have been carried out with Argon and Helium as background gas. The emission spectrum of these plasmas in the actively heated case is dominated by the InBr band (A − X and B − X transition) and by atomic indium lines arising from the dissociation of InBr whereas the emission from the background gas only plays a minor role. Figure 5 shows exemplary two measured spectra of InBr with different external parameters (different heating temperature, type and pressure of background gas) and the simulation which gives the best fit to the measurement. It can be seen that the structure of the band spectrum, and therefore T_{Vib} and T_{Rot}, varies strongly. The simulation

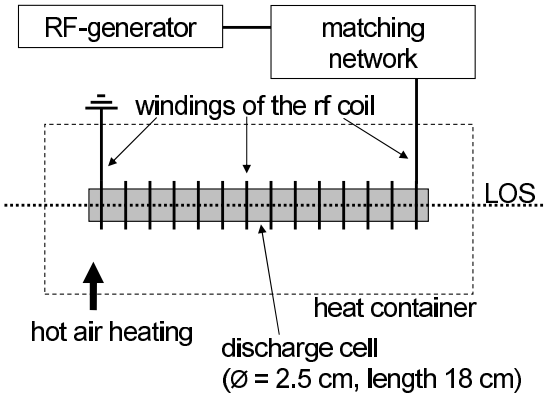

Figure 4. Sketch of the experimental setup.

matches the measurement in both cases very well what proves that the application of the Hönl-London factors of Hund's case (a) in the calculation of the intensity distribution of the rotational lines is reasonable (see section 2.1). The vibrational and rotational temperatures can be determined with small errors ($\Delta T_{\mathrm{Vib}} = \pm 100$ K, $\Delta T_{\mathrm{Rot}} = \pm 50$ K). As one could hardly distinguish the measurement from the simulation due to the good match, the measurements in figure 5 are baseline-shifted for better visibility.

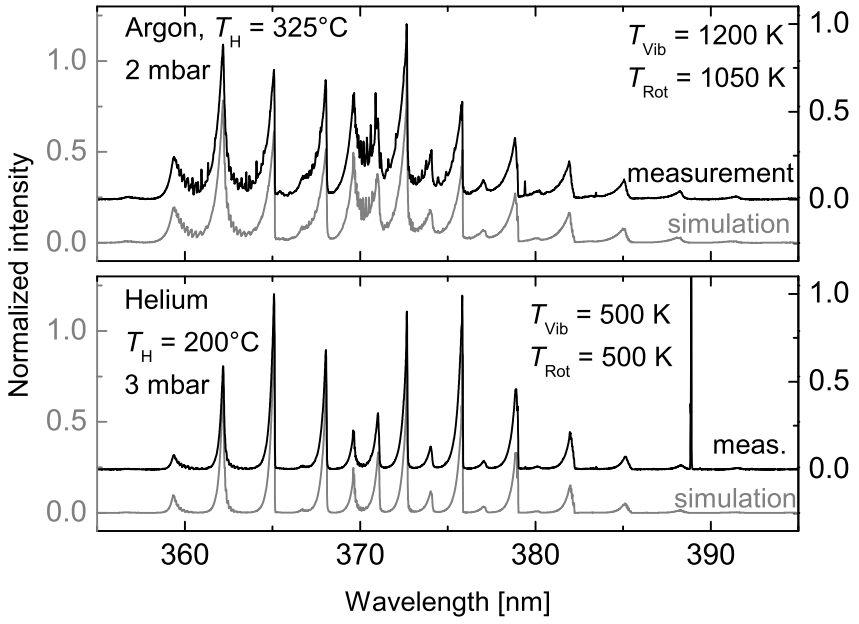

Figure 5. Measured band spectra of InBr in Argon (upper part) and Helium (bottom part). The InBr emission in Helium is overlapped by Helium emission lines. For a better visibility the measured spectrum is baseline-shifted.

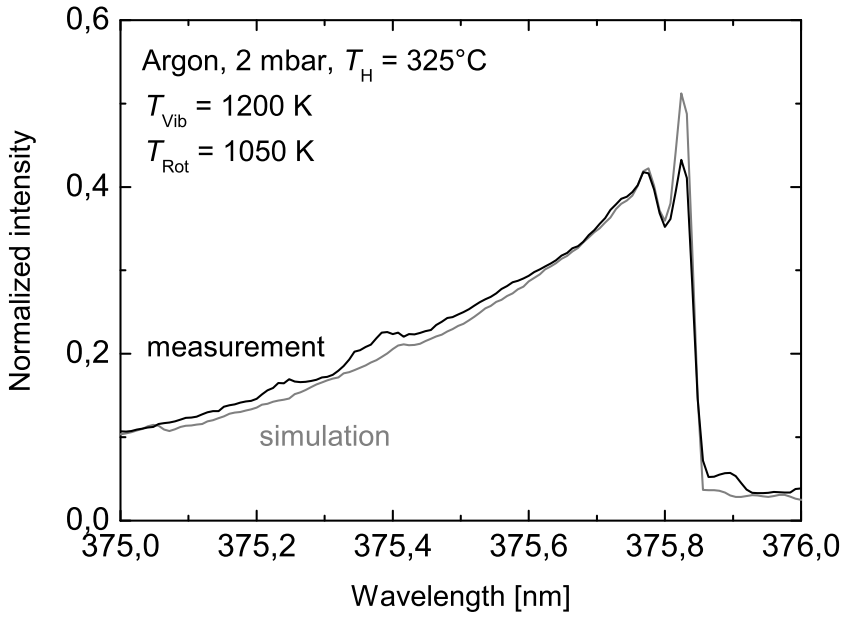

Figure 6. Simulation and measurement of the $\Delta v = +1$ sequence of the A − X transition.

Figure 6 shows the $\Delta v = 0$ sequence of the A − X transition of the measurement in Argon and the appendant simulation in detail. The double peak structure of the sequence is well reproduced. In literature [8], however, it was discussed if this "asymmetric shape" is caused by population transfer out of metastable states into certain vibrational levels. Since the simulation presented in this paper is only based on molecular constants, such transfer mechanism seems not to be the cause for the double peak structure.

3.3. Determination of the InBr density

An important parameter of InBr discharges which strongly influences the intensity of the band emission is the ground state density of the molecule. It is determined by the coldest spot of the wall of the quartz cell which is not well-defined in this experimental setup. However, the ground state density of InBr can be derived from absorption spectroscopy measurements using the effective transition probabilities A_{ik}^{eff} of the A − X or the B − X transition. As shown in section 2.3 the calculation of the A_{ik}^{eff} needs the vibrational temperature of InBr as input parameter which is gained from adjusting the simulation to the measured band spectrum. If the amount of InBr is very high, reabsorption of the intense sequences in the emission spectrum occurs. This can distort the shape of the spectrum drastically as shown in figure 7 and make a determination of the vibrational and rotational temperature with the simulation program impossible. In this case, however, the ground state density of InBr can still be obtained via absorption

spectroscopy by using only the B − X transition since the effective transition probability $A^{\text{eff}}_{\text{BX}}$ is almost constant for all vibrational temperatures.

For low densities of InBr, which means negligible reabsorption effects, the A and the B state can both be analyzed using the individual effective transition probabilities. The resulting densities differ only by a few percent. Therefore it is reasonable to use only the B − X transition for the determination of the ground state density of InBr via absorption spectroscopy.

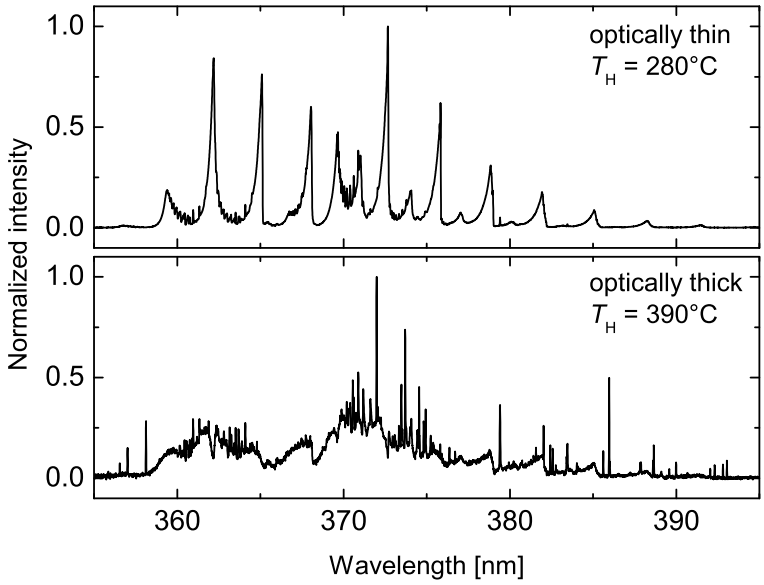

Figure 7. Examples of the emission band structure of InBr without (upper part) and with reabsorption caused by high InBr ground state densities at high heating temperatures (bottom part).

To compare the population density of the ground state determined via absorption spectroscopy to the density calculated from an Arrhenius type vapour pressure equation [8], the lowest temperature measured by the three thermocouples T_{low} was used as an approximation for the coldest spot temperature (see table 4). Figure 8 shows measured densities in a discharge with Argon as background gas as a function of the heating temperature. A very good agreement is observed at high T_{H}. For low heating temperatures the difference between the values obtained by the two methods increases. At $T_{\text{H}} = 300$ °C the deviation is about a factor 4 which indicates that the approximation of using the heating temperature as coldest spot temperature is only valid for high heating temperature values. The distance between the thermocouple and the discharge cell is a few centimeter. Therefore the measured heating temperature can underestimate the cold spot temperature due to temperature gradients occurring especially for low heating temperatures.

Table 4. Heating temperature and the lowest measured temperature inside the heat container which is used as an approximation for the coldest spot temperature.

T_{H} (K)	T_{low} (K)
299	269
324	288
346	298
362	319
377	337
390	356

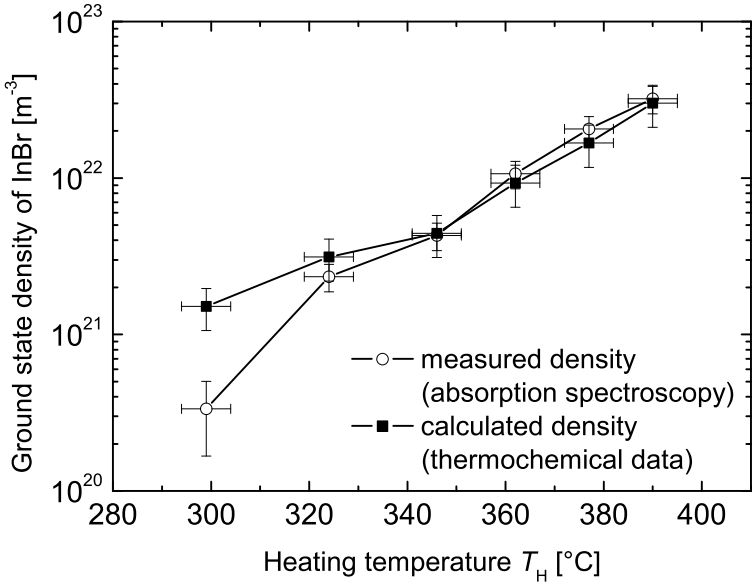

Figure 8. Ground state density of InBr with increasing heating temperature T_{H} of the cell determined on the one hand with absorption spectroscopy (using only the B − X transition) and on the other hand with the vapour pressure equation [8] using the lowest temperature measured by the three thermocouples T_{low} as approximation for the coldest spot of the cell wall.

4. Conclusion

Recent research in lighting technology focuses on finding efficient substitutes for mercury in low and high pressure lamps due to the toxicity of Hg. Metal halides such as InBr are discussed as an efficient molecular radiator in low pressure plasmas. Thus, low pressure rare gas discharges containing InBr have been investigated spectroscopically with focus on the near UV band emission arising from the A $^3\Pi_{0^+} \rightarrow$ X $^1\,\Sigma_0^+$ and the B $^3\Pi_1 \rightarrow$ X $^1\Sigma_0^+$ transitions. The absolute intensity of this emission strongly depends on the amount of InBr in the plasma whereas the relative intensity is determined by the vibrational

and rotational population of the electronic states. To determine these populations, the relative band emission has been simulated using Boltzmann distributions for the vibrational and rotational states. The simulation requires a complete set of Franck-Condon factors and vibrationally resolved transition probabilities which was not available in literature so far. Therefore this data has been derived by applying the Schrödinger equation to Born-Oppenheimer potential curves of the X, A and B states of InBr. The simulation matches the measured spectra very well; the vibrational and rotational temperature of the molecule are used as fitting parameters. The dependencies of the spectra on vibrational and rotational temperature have been demonstrated. Using high resolution measurements, these temperatures can be determined with high accuracy. It has been pointed out that the simulation is not applicable if reabsorption of the emission distorts the shape of the band spectrum. Knowing the vibrational temperature, an effective transition probability for the electronic A − X or B − X transition can be calculated. For the A state, the transition probability changes with varying T_{Vib} whereas the transition probability of the B state is nearly independent of the vibrational temperature. Using these transition probabilities together with white light absorption spectroscopy measurements the ground state density of InBr in the plasma has been determined. Even if the emission spectra are influenced by reabsorption effects, the B − X transition can still be used to determine the InBr ground state density. The results are in good agreement with the densities calculated from an Arrhenius type vapour pressure equation and are independent on the knowledge of any experimental parameters such as the temperature of the coldest spot of the discharge cell wall.

In summary, it has been demonstrated that the simulation of the relative intensity of the emission spectrum of InBr allows the determination of the vibrational and rotational temperature of the molecule in optically thin low pressure plasmas and the ground state density of InBr via absorption spectroscopy with high sensitivity.

Acknowledgments

The authors would like to thank Dirk Wünderlich from the Max-Planck-Institut für Plasma Physik in Garching, Germany, for his kind assistance in using the TraDiMo package.

References

[1] Uhrlandt D, Bussiahn R, Gorchakov S, Lange H, Loffhagen D and Nötzold D 2005 *J. Phys. D: Appl. Phys.* **38** 3318–25
[2] Jinno M, Kurokawa H and Aono M 1999 *Japan. J. Appl. Phys.* **38** 4608–12
[3] Jinno M, Kurokawa H and Aono M 1999 *Japan. J. Appl. Phys.* **38** 4613–7
[4] Born M 2002 *Plasma Sources Sci. Technol.* **11** A55–A63
[5] Franke St, Methling R, Hess H, Schneidenbach H, Schöpp H, Hitzschke L, Käning M and Schalk B 2007 *J. Phys. D: Appl. Phys.* **40** 3836–41
[6] Kitsinelis S, Zissis G and Fokitis E 2009 *J. Phys. D: Appl. Phys.* **42** 045209
[7] Waymouth J F 1971 *Electric Discharge Lamps* (MIT Press, Cambridge MA)

[8] Körber A and Hayashi D 2007 *XXVIII Int. Conf. on Phenomena in Ionized Gases (Prague)*
[9] Hayashi D, Hilbig R, Körber A, Schwan S, Scholl R, Boerger M and Huppertz M 2010 *Appl. Phys. Lett.* **96** 061503
[10] Mishra S K, Yadav R K S, Singh V B and Rai S B 2004 *J. Phys. Chem. Ref. Data* **33** 453–70
[11] Banerjee A, Pramanik A, Chakrabarti S and Das K K 2009 *Journal of Molecular Structure: THEOCHEM* **893** 37–47
[12] Wehrli M and Miescher E 1934 *Helv. Phys. Acta* **7** 289–330
[13] Berkowitz J and Dehmer J L 1972 *J. Chem. Phys.* **57** 3194–3201
[14] Fantz U 2006 *Plasma Sources Sci. Technol.* **15** S137–S147
[15] Fantz U and Heger B 1998 *Plasma Phys. Control. Fusion* **40** 2023–32
[16] Herzberg G 1950 *Molecular Spectra and Molecular Structure: I. Spectra of Diatomic Molecules* (D. van Nostrand, New York)
[17] Kovács I 1969 *Rotational Structure in the Spectra of Diatomic Molecules* (Adam Hilger LTD, London)
[18] Singh V B, Rai A K, Rai S B and Rai D K 1988 *Indian J. Phys.* **62B** 41–46
[19] Fantz U and Wünderlich D 2006 *Atomic Data and Nuclear Data Tables* **92** 853–973
[20] Mishra S K, Yadav R K S, Rai S B and Singh V B 2003 *Indian J. Phys.* **77B** 229–32

Appendix

Table A1. Franck-Condon factors for the A − X transition, part 1 (from $v'' = 0$ to $v'' = 12$).

v'	$v'' = 0$	$v'' = 1$	$v'' = 2$	$v'' = 3$	$v'' = 4$	$v'' = 5$	$v'' = 6$	$v'' = 7$	$v'' = 8$	$v'' = 9$	$v'' = 10$	$v'' = 11$	$v'' = 12$
0	0.581 82	0.293 43	0.094 45	0.024 06	0.005 09	0.000 98	0.000 16	0.000 02	0	0	0	0	0
1	0.343 17	0.136 01	0.279 79	0.161 50	0.058 67	0.016 24	0.003 75	0.000 73	0.000 13	0.000 02	0	0	0
2	0.069 79	0.407 45	0.011 62	0.193 27	0.185 00	0.090 80	0.031 16	0.008 56	0.001 90	0.000 37	0.000 06	0.000 01	0
3	0.005 10	0.148 56	0.371 48	0.003 81	0.112 48	0.178 04	0.113 60	0.047 24	0.014 91	0.003 80	0.000 81	0.000 14	0.000 02
4	0.000 06	0.014 48	0.216 36	0.310 20	0.028 53	0.056 41	0.155 35	0.126 29	0.061 87	0.022 33	0.006 29	0.001 49	0.000 28
5	0	0.000 14	0.025 92	0.269 61	0.252 26	0.054 54	0.023 40	0.127 82	0.130 14	0.073 97	0.029 93	0.009 30	0.002 39
6	0	0.000 02	0.000 18	0.037 30	0.310 36	0.206 49	0.072 50	0.006 92	0.101 44	0.127 65	0.083 02	0.037 12	0.012 62
7	0	0	0.000 08	0.000 13	0.047 00	0.341 90	0.173 91	0.081 46	0.000 74	0.078 81	0.121 39	0.088 98	0.043 63
8	0	0	0	0.000 21	0.000 03	0.053 87	0.367 15	0.153 10	0.083 03	0.000 29	0.060 77	0.113 05	0.092 46
9	0	0	0	0	0.000 45	0.000 03	0.057 17	0.388 05	0.142 25	0.079 27	0.002 65	0.047 03	0.104 13
10	0	0	0	0	0	0.000 82	0.000 42	0.056 45	0.405 51	0.139 93	0.071 91	0.006 13	0.037 00
11	0	0	0	0	0	0	0.001 29	0.001 61	0.051 66	0.419 48	0.145 22	0.062 25	0.009 86
12	0	0	0	0	0	0	0	0.001 81	0.004 05	0.043 16	0.429 09	0.157 67	0.051 23
13	0	0	0	0	0	0	0.000 02	0	0.002 25	0.008 16	0.031 89	0.432 58	0.177 08
14	0	0	0	0	0	0	0	0.000 03	0.000 06	0.002 46	0.014 19	0.019 44	0.427 80
15	0	0	0	0	0	0	0	0	0.000 05	0.000 20	0.002 30	0.021 98	0.008 14
16	0	0	0	0	0	0	0	0	0	0.000 05	0.000 49	0.001 71	0.030 91
17	0	0	0	0	0	0	0	0	0	0	0.000 05	0.000 97	0.000 83
18	0	0	0	0	0	0	0	0	0	0	0.000 02	0.000 03	0.001 62
19	0	0	0	0	0	0	0	0	0	0	0	0.000 04	0
20	0	0	0	0	0	0	0	0	0	0	0	0	0.000 07
21	0	0	0	0	0	0	0	0	0	0	0	0	0
22	0	0	0	0	0	0	0	0	0	0	0	0	0
23	0	0	0	0	0	0	0	0	0	0	0	0	0
24	0	0	0	0	0	0	0	0	0	0	0	0	0

Table A2. Franck-Condon factors for the A − X transition, part 2 (from $v'' = 13$ to $v'' = 24$).

v'	$v'' = 13$	$v'' = 14$	$v'' = 15$	$v'' = 16$	$v'' = 17$	$v'' = 18$	$v'' = 19$	$v'' = 20$	$v'' = 21$	$v'' = 22$	$v'' = 23$	$v'' = 24$
0	0	0	0	0	0	0	0	0	0	0	0	0
1	0	0	0	0	0	0	0	0	0	0	0	0
2	0	0	0	0	0	0	0	0	0	0	0	0
3	0	0	0	0	0	0	0	0	0	0	0	0
4	0.000 04	0	0	0	0	0	0	0	0	0	0	0
5	0.000 49	0.000 08	0.000 01	0	0	0	0	0	0	0	0	0
6	0.003 47	0.000 76	0.000 14	0.000 02	0	0	0	0	0	0	0	0
7	0.015 95	0.004 71	0.001 09	0.000 21	0.000 03	0	0	0	0	0	0	0
8	0.049 01	0.019 25	0.005 98	0.001 46	0.000 29	0.000 04	0	0	0	0	0	0
9	0.093 80	0.053 38	0.022 20	0.007 28	0.001 86	0.000 38	0.000 05	0	0	0	0	0
10	0.095 37	0.093 69	0.056 61	0.024 84	0.008 49	0.002 26	0.000 48	0.000 07	0	0	0	0
11	0.029 95	0.087 29	0.092 56	0.058 88	0.027 03	0.009 60	0.002 64	0.000 58	0.000 08	0	0	0
12	0.013 51	0.025 30	0.080 08	0.090 79	0.060 27	0.028 72	0.010 56	0.002 98	0.000 67	0.000 10	0	0
13	0.039 62	0.017 03	0.022 57	0.073 71	0.088 83	0.060 80	0.030 03	0.011 27	0.003 30	0.000 73	0.000 11	0
14	0.203 12	0.028 14	0.020 54	0.021 48	0.068 16	0.086 76	0.060 71	0.030 83	0.011 82	0.003 52	0.000 79	0.000 12
15	0.412 34	0.235 10	0.017 55	0.024 29	0.021 93	0.063 22	0.084 87	0.060 03	0.031 21	0.012 16	0.003 66	0.000 83
16	0.000 98	0.384 04	0.271 57	0.008 71	0.028 53	0.023 98	0.058 67	0.083 30	0.058 83	0.031 21	0.012 30	0.003 72
17	0.039 70	0.001 30	0.341 73	0.309 99	0.002 57	0.033 58	0.027 92	0.054 21	0.082 26	0.057 06	0.030 94	0.012 17
18	0.000 10	0.046 55	0.012 16	0.285 91	0.346 58	0.000 03	0.039 71	0.034 18	0.049 62	0.081 86	0.054 80	0.030 37
19	0.002 34	0.000 24	0.049 36	0.035 49	0.219 57	0.376 44	0.001 72	0.047 11	0.043 43	0.044 61	0.082 31	0.051 96
20	0.000 02	0.002 89	0.002 20	0.046 46	0.070 99	0.148 64	0.393 86	0.007 73	0.055 79	0.056 49	0.038 98	0.083 84
21	0.000 09	0.000 17	0.003 00	0.006 76	0.037 30	0.115 22	0.081 84	0.393 35	0.017 34	0.065 47	0.074 25	0.032 63
22	0	0.000 09	0.000 52	0.002 45	0.014 17	0.023 47	0.161 23	0.029 65	0.370 98	0.028 78	0.075 30	0.097 51
23	0	0.000 03	0.000 06	0.001 15	0.001 34	0.023 58	0.009 07	0.199 19	0.002 29	0.325 86	0.039 40	0.083 89
24	0	0	0.000 05	0.000 01	0.001 95	0.000 23	0.032 78	0.000 43	0.218 25	0.006 58	0.261 50	0.046 16

Table A3. Franck-Condon factors for the B − X transition, part 1 (from $v'' = 0$ to $v'' = 12$).

v'	$v''=0$	$v''=1$	$v''=2$	$v''=3$	$v''=4$	$v''=5$	$v''=6$	$v''=7$	$v''=8$	$v''=9$	$v''=10$	$v''=11$	$v''=12$
0	0.620 75	0.273 90	0.081 30	0.019 31	0.003 91	0.000 71	0.000 11	0.000 02	0	0	0	0	0
1	0.323 54	0.188 19	0.280 95	0.143 61	0.047 98	0.012 42	0.002 72	0.000 49	0.000 08	0.000 01	0	0	0
2	0.053 26	0.415 06	0.038 24	0.214 52	0.171 66	0.075 56	0.024 00	0.006 15	0.001 29	0.000 24	0.000 04	0	0
3	0.002 44	0.116 23	0.414 97	0.001 41	0.143 97	0.173 83	0.096 79	0.036 50	0.010 74	0.002 51	0.000 51	0.000 08	0.000 01
4	0	0.006 58	0.173 40	0.385 53	0.004 17	0.089 00	0.161 54	0.110 22	0.048 38	0.015 93	0.004 17	0.000 91	0.000 16
5	0	0.000 01	0.010 95	0.220 73	0.352 93	0.016 30	0.051 46	0.143 15	0.116 93	0.058 38	0.021 33	0.006 07	0.001 44
6	0	0.000 04	0.000 08	0.014 28	0.258 26	0.327 32	0.026 62	0.027 76	0.123 93	0.118 42	0.066 21	0.026 45	0.008 11
7	0	0	0.000 10	0.000 37	0.015 69	0.286 94	0.311 97	0.031 90	0.013 69	0.106 60	0.116 33	0.071 95	0.030 92
8	0	0	0	0.000 22	0.001 09	0.014 78	0.307 50	0.307 36	0.032 12	0.005 86	0.092 19	0.112 19	0.075 64
9	0	0	0	0	0.000 37	0.002 55	0.011 71	0.319 89	0.313 09	0.028 28	0.001 88	0.081 11	0.106 82
10	0	0	0	0	0	0.000 50	0.005 00	0.007 20	0.323 32	0.328 26	0.021 80	0.000 25	0.073 24
11	0	0	0	0	0	0.000 03	0.000 56	0.008 58	0.002 65	0.316 53	0.351 61	0.014 15	0.000 07
12	0	0	0	0	0	0	0.000 09	0.000 48	0.013 14	0.000 07	0.298 14	0.381 21	0.006 89
13	0	0	0	0	0	0	0	0.000 22	0.000 26	0.018 17	0.001 95	0.267 23	0.414 25
14	0	0	0	0	0	0	0	0	0.000 42	0.000 03	0.022 67	0.010 87	0.224 11
15	0	0	0	0	0	0	0	0	0	0.000 69	0.000 11	0.025 30	0.028 79
16	0	0	0	0	0	0	0	0	0.000 01	0	0.000 95	0.001 02	0.024 78
17	0	0	0	0	0	0	0	0	0	0.000 02	0.000 05	0.001 09	0.003 31
18	0	0	0	0	0	0	0	0	0	0	0.000 02	0.000 16	0.000 95
19	0	0	0	0	0	0	0	0	0	0	0	0.000 02	0.000 40
20	0	0	0	0	0	0	0	0	0	0	0	0.000 01	0
21	0	0	0	0	0	0	0	0	0	0	0	0	0.000 02
22	0	0	0	0	0	0	0	0	0	0	0	0	0
23	0	0	0	0	0	0	0	0	0	0	0	0	0
24	0	0	0	0	0	0	0	0	0	0	0	0	0

Table A4. Franck-Condon factors for the B − X transition, part 2 (from $v'' = 13$ to $v'' = 24$).

v'	$v'' = 13$	$v'' = 14$	$v'' = 15$	$v'' = 16$	$v'' = 17$	$v'' = 18$	$v'' = 19$	$v'' = 20$	$v'' = 21$	$v'' = 22$	$v'' = 23$	$v'' = 24$
0	0	0	0	0	0	0	0	0	0	0	0	0
1	0	0	0	0	0	0	0	0	0	0	0	0
2	0	0	0	0	0	0	0	0	0	0	0	0
3	0	0	0	0	0	0	0	0	0	0	0	0
4	0.000 02	0	0	0	0	0	0	0	0	0	0	0
5	0.000 26	0.000 04	0	0	0	0	0	0	0	0	0	0
6	0.002 05	0.000 40	0.000 06	0.000 01	0	0	0	0	0	0	0	0
7	0.010 20	0.002 69	0.000 56	0.000 09	0.000 01	0	0	0	0	0	0	0
8	0.034 74	0.012 09	0.003 37	0.000 72	0.000 13	0.000 01	0	0	0	0	0	0
9	0.077 80	0.037 65	0.013 80	0.003 98	0.000 89	0.000 16	0.000 02	0	0	0	0	0
10	0.100 97	0.078 70	0.039 78	0.015 17	0.004 55	0.001 03	0.000 19	0.000 02	0	0	0	0
11	0.068 45	0.094 87	0.078 80	0.041 05	0.016 26	0.004 99	0.001 17	0.000 21	0.000 02	0	0	0
12	0.000 91	0.066 61	0.088 68	0.078 37	0.041 56	0.017 00	0.005 31	0.001 26	0.000 23	0.000 02	0	0
13	0.001 67	0.002 63	0.067 75	0.082 33	0.077 72	0.041 34	0.017 41	0.005 49	0.001 33	0.000 23	0.000 02	0
14	0.446 64	0.000 04	0.005 28	0.072 09	0.075 64	0.077 12	0.040 42	0.017 54	0.005 52	0.001 35	0.000 23	0.000 02
15	0.171 19	0.472 99	0.003 37	0.009 05	0.080 06	0.068 37	0.076 85	0.038 80	0.017 42	0.005 42	0.001 34	0.000 22
16	0.056 16	0.113 50	0.486 94	0.012 40	0.014 14	0.092 30	0.060 29	0.077 21	0.036 49	0.017 11	0.005 17	0.001 29
17	0.020 37	0.090 99	0.059 02	0.481 94	0.026 87	0.020 62	0.109 55	0.051 27	0.078 54	0.033 45	0.016 70	0.004 81
18	0.007 31	0.012 74	0.128 07	0.017 80	0.452 86	0.045 13	0.028 27	0.132 58	0.041 31	0.081 27	0.029 63	0.016 30
19	0.000 54	0.012 73	0.004 44	0.159 42	0.000 14	0.397 74	0.063 98	0.036 32	0.161 80	0.030 77	0.085 84	0.025 04
20	0.000 73	0.000 08	0.018 40	0.000 02	0.175 59	0.013 49	0.319 58	0.079 08	0.043 32	0.196 89	0.020 31	0.092 79
21	0	0.001 09	0.000 16	0.022 18	0.004 91	0.168 81	0.058 90	0.227 33	0.085 97	0.047 16	0.236 21	0.010 98
22	0.000 03	0.000 06	0.001 26	0.001 67	0.021 85	0.023 22	0.136 97	0.128 23	0.135 18	0.081 60	0.045 56	0.276 21
23	0	0.000 03	0.000 24	0.001 06	0.005 26	0.016 35	0.054 72	0.086 94	0.203 64	0.059 29	0.066 02	0.037 18
24	0	0.000 02	0.000 01	0.000 57	0.000 48	0.010 77	0.007 44	0.092 44	0.034 97	0.261 56	0.012 73	0.043 21

Table A5. Transition probabilities $A_{ik}^{v'v''}$ (s^{-1}) for the A − X transition, part 1 (from $v'' = 0$ to $v'' = 12$).

v'	$v''=0$	$v''=1$	$v''=2$	$v''=3$	$v''=4$	$v''=5$	$v''=6$	$v''=7$	$v''=8$	$v''=9$	$v''=10$	$v''=11$	$v''=12$
0	951 37	388 24	103 29	2187	377	60	8	1	0	0	0	0	0
1	684 98	233 14	374 00	177 91	5353	1216	230	35	5	0	0	0	0
2	174 19	831 20	2400	261 17	204 95	8324	2341	527	91	14	2	0	0
3	1717	377 96	777 46	346	153 78	198 29	104 33	3568	916	184	30	4	0
4	40	5011	561 53	669 29	3755	7822	173 71	116 24	4673	1377	303	56	7
5	0	118	9240	714 46	564 44	7525	3303	143 46	119 79	5588	1844	448	89
6	0	4	198	137 29	840 56	482 19	100 58	1002	114 27	117 28	6268	2278	609
7	0	1	16	233	179 20	947 15	426 35	111 39	114	8910	111 19	6694	2672
8	0	0	3	51	197	213 63	1041 20	395 74	109 89	38	6909	102 94	6933
9	0	0	0	6	123	100	237 07	1127 10	388 21	9942	391	5391	9408
10	0	0	0	0	9	251	9	246 78	1206 80	402 47	8293	958	4301
11	0	0	0	0	1	11	443	51	240 86	1279 50	438 14	6308	1638
12	0	0	0	0	0	2	8	692	407	218 75	1341 40	495 71	4219
13	0	0	0	0	0	0	6	3	964	1290	181 60	1385 90	575 92
14	0	0	0	0	0	0	0	13	1	1200	2897	133 16	1404 60
15	0	0	0	0	0	0	0	0	23	18	1320	5336	8012
16	0	0	0	0	0	0	0	0	0	33	82	1243	8555
17	0	0	0	0	0	0	0	0	1	1	38	224	944
18	0	0	0	0	0	0	0	0	0	1	6	36	463
19	0	0	0	0	0	0	0	0	0	0	1	13	21
20	0	0	0	0	0	0	0	0	0	0	0	0	27
21	0	0	0	0	0	0	0	0	0	0	0	0	0
22	0	0	0	0	0	0	0	0	0	0	0	0	1
23	0	0	0	0	0	0	0	0	0	0	0	0	0
24	0	0	0	0	0	0	0	0	0	0	0	0	0

Table A6. Transition probabilities $A_{ik}^{v'v''}$ (s^{-1}) for the A − X transition, part 2 (from $v'' = 13$ to $v'' = 24$).

v'	$v''=13$	$v''=14$	$v''=15$	$v''=16$	$v''=17$	$v''=18$	$v''=19$	$v''=20$	$v''=21$	$v''=22$	$v''=23$	$v''=24$
0	0	0	0	0	0	0	0	0	0	0	0	0
1	0	0	0	0	0	0	0	0	0	0	0	0
2	0	0	0	0	0	0	0	0	0	0	0	0
3	0	0	0	0	0	0	0	0	0	0	0	0
4	1	0	0	0	0	0	0	0	0	0	0	0
5	12	1	0	0	0	0	0	0	0	0	0	0
6	128	19	2	0	0	0	0	0	0	0	0	0
7	765	174	26	3	0	0	0	0	0	0	0	0
8	2980	922	218	36	4	0	0	0	0	0	0	0
9	6992	3227	1053	264	44	5	0	0	0	0	0	0
10	8518	6941	3389	1170	303	53	7	0	0	0	0	0
11	3563	7675	6807	3487	1258	337	61	8	0	0	0	0
12	2410	3118	6893	6624	3524	1318	366	66	9	0	0	0
13	2277	3309	2932	6157	6440	3492	1364	378	73	8	0	0
14	678 57	766	4409	2991	5465	6257	3419	1378	387	75	8	0
15	1387 30	801 62	23	5823	3324	4786	6108	3299	1371	388	75	8
16	3264	1324 10	939 84	429	7699	4001	4093	6017	3136	1346	381	71
17	122 42	345	1208 00	1083 50	2368	102 30	5152	3357	6021	2917	1318	359
18	484	158 22	638	1037 50	1217 80	6147	136 23	6962	2571	6146	2651	1280
19	796	78	184 48	5308	820 18	1323 60	118 71	180 93	9706	1745	6447	2325
20	3	1153	78	192 40	148 82	575 04	1378 40	192 94	237 82	137 23	941	6993
21	43	7	1427	916	175 22	287 94	332 87	1361 30	277 02	306 78	194 10	285
22	1	57	77	1458	2940	132 68	450 68	133 20	1258 50	358 16	384 61	271 37
23	1	5	57	263	1162	6178	7445	603 65	1687	1069 40	419 43	464 04
24	0	1	16	39	583	597	101 11	2114	704 84	1364	812 57	443 05

Table A7. Transition probabilities $A_{ik}^{v'v''}$ (s^{-1}) for the B − X transition, part 1 (from $v'' = 0$ to $v'' = 12$).

v'	$v''=0$	$v''=1$	$v''=2$	$v''=3$	$v''=4$	$v''=5$	$v''=6$	$v''=7$	$v''=8$	$v''=9$	$v''=10$	$v''=11$	$v''=12$
0	679 97	292 74	8478	1965	388	68	10	1	0	0	0	0	0
1	363 15	206 15	300 31	149 79	4883	1232	263	47	8	1	0	0	0
2	6122	465 74	4188	229 28	179 05	7690	2383	595	121	22	3	0	0
3	288	133 54	465 43	155	153 84	181 28	9851	3625	1041	238	47	7	1
4	0	773	199 08	432 13	456	9507	168 42	112 15	4804	1543	394	84	14
5	1	1	1287	253 19	395 28	1783	5494	149 18	118 94	5796	2067	574	133
6	0	4	10	1675	295 92	366 24	2908	2961	129 07	120 40	6571	2562	767
7	0	0	13	44	1838	328 38	348 67	3482	1459	110 93	118 19	7136	2994
8	0	0	0	27	131	1729	351 42	343 08	3501	624	9584	113 88	7497
9	0	0	0	0	45	304	1367	365 00	348 97	3079	200	8422	108 33
10	0	0	0	0	1	61	596	840	368 28	365 28	2369	26	7595
11	0	0	0	0	1	4	68	1021	308	359 87	390 56	1535	7
12	0	0	0	0	0	1	11	58	1561	8	338 26	422 61	747
13	0	0	0	0	0	0	1	27	31	2153	226	302 51	458 25
14	0	0	0	0	0	0	0	1	52	3	2679	1256	253 10
15	0	0	0	0	0	0	0	1	0	86	14	2983	3318
16	0	0	0	0	0	0	0	0	2	1	117	123	2913
17	0	0	0	0	0	0	0	0	0	3	6	133	396
18	0	0	0	0	0	0	0	0	0	0	3	20	116
19	0	0	0	0	0	0	0	0	0	0	1	2	49
20	0	0	0	0	0	0	0	0	0	0	0	2	1
21	0	0	0	0	0	0	0	0	0	0	0	0	3
22	0	0	0	0	0	0	0	0	0	0	0	0	0
23	0	0	0	0	0	0	0	0	0	0	0	0	0
24	0	0	0	0	0	0	0	0	0	0	0	0	0

Table A8. Transition probabilities $A_{ik}^{v'v''}$ (s^{-1}) for the B − X transition, part 2 (from $v'' = 13$ to $v'' = 24$).

v'	$v'' = 13$	$v'' = 14$	$v'' = 15$	$v'' = 16$	$v'' = 17$	$v'' = 18$	$v'' = 19$	$v'' = 20$	$v'' = 21$	$v'' = 22$	$v'' = 23$	$v'' = 24$
0	0	0	0	0	0	0	0	0	0	0	0	0
1	0	0	0	0	0	0	0	0	0	0	0	0
2	0	0	0	0	0	0	0	0	0	0	0	0
3	0	0	0	0	0	0	0	0	0	0	0	0
4	2	0	0	0	0	0	0	0	0	0	0	0
5	24	4	0	0	0	0	0	0	0	0	0	0
6	189	36	6	1	0	0	0	0	0	0	0	0
7	964	248	50	8	1	0	0	0	0	0	0	0
8	3361	1142	311	65	11	1	0	0	0	0	0	0
9	7704	3640	1303	367	80	14	1	0	0	0	0	0
10	102 27	7785	3843	1431	419	93	16	1	0	0	0	0
11	7088	9596	7784	3961	1532	459	105	19	2	0	0	0
12	96	6886	8956	7731	4005	1600	488	113	20	2	0	0
13	180	277	6991	8300	7655	3977	1636	504	119	21	2	0
14	492 95	5	557	7424	7611	7582	3882	1646	506	121	20	2
15	192 83	520 74	363	952	8227	6865	7540	3720	1631	496	120	19
16	6454	127 50	534 69	1331	1483	9462	6040	7559	3491	1600	473	115
17	2387	104 25	6611	527 71	2876	2157	112 03	5124	7672	3193	1558	438
18	874	1488	146 27	1988	494 39	4817	2949	135 21	4119	7918	2822	1517
19	66	1516	517	181 47	16	432 85	6808	3778	164 54	3059	8341	2378
20	91	9	2182	3	199 17	1497	34663	8387	4492	199 62	2014	8992
21	0	134	20	2620	568	190 78	6511	24572	9087	4874	238 71	1085
22	4	8	154	201	2571	2673	154 21	141 20	145 58	8594	4692	278 19
23	1	3	30	129	630	1916	6273	9749	223 36	6361	6927	3815
24	0	2	1	71	59	1284	868	10552	3904	285 70	1360	4516